

Mercury's sodium exosphere: Magnetospheric ion recycling

F. Leblanc

Service d'Aéronomie du CNRS/IPSL, Verrières-Le-Buisson, France

D. Delcourt

Centre d'Etudes des Environnements Terrestre et Planétaires/IPSL, Saint Maur, France

R. E. Johnson

Engineering Physics Program, University of Virginia, Charlottesville, Virginia, USA

Received 9 July 2003; revised 29 August 2003; accepted 11 September 2003; published 19 December 2003.

[1] A three-dimensional Monte Carlo model of Mercury's neutral sodium exosphere was used to describe correlation between the observed variations in the exospheric density and the variations in the surface concentration of sodium along Mercury's motion around the Sun [Leblanc and Johnson, 2003]. Four processes of ejection were taken into account: thermal and photon stimulated desorptions, solar wind sputtering, and micrometeoroid vaporization. Here a model of ion circulation in Mercury's magnetosphere developed by Delcourt *et al.* [2002, 2003] is used to examine the contribution from sodium magnetospheric ion recycling. The model is coupled to the exospheric model to track newly ionized sodium formed in Mercury's exosphere. The coupled Na and Na⁺ model is used to examine the sputtering by and implantation of the reimpacting ions. The magnetospheric ion sputtering does not contribute significantly to the total amount of Na atoms ejected into Mercury's exosphere because of its rather small flux; however, magnetospheric ion implantation in Mercury's surface is sufficiently concentrated inside narrow latitude bands to enhance the local surface concentration of sodium. This enhancement is seen to contribute to the peaks in Mercury's exospheric sodium emission observed at high latitudes when the implanted sodium is exposed to the solar flux near the dayside terminator. *INDEX TERMS:* 6235 Planetology: Solar System Objects: Mercury; 2736 Magnetospheric Physics: Magnetosphere/ionosphere interactions; 5409 Planetology: Solid Surface Planets: Atmospheres—structure and dynamics; 5415 Planetology: Solid Surface Planets: Erosion and weathering; 7807 Space Plasma Physics: Charged particle motion and acceleration; *KEYWORDS:* Mercury, atmosphere, dynamic, magnetosphere

Citation: Leblanc, F., D. Delcourt, and R. E. Johnson, Mercury's sodium exosphere: Magnetospheric ion recycling, *J. Geophys. Res.*, 108(E12), 5136, doi:10.1029/2003JE002151, 2003.

1. Introduction

[2] Mariner 10, the only spacecraft which has ever been close enough to Mercury to obtain in situ measurements, provided evidence for the presence of a significant intrinsic magnetic field [Ness *et al.*, 1974]. The magnetic field structure revealed by the Mariner 10 magnetometer and plasma instruments supports the assumption that Mercury's magnetic field is similar in structure to the Earth's magnetic field [Connerney and Ness, 1988; Luhmann *et al.*, 1998]. Mariner 10 airglow spectrometer and occultation experiments observed only few elements of Mercury's exosphere [Broadfoot *et al.*, 1976]. It provided spatial and energy distributions for H and He elements, a "very uncertain" density for O atoms at the subsolar point and indicated that the total density at the subsolar point is less than

10^7 particles/cm³ [Broadfoot *et al.*, 1976]. The largest set of information about Mercury's exosphere, its structure, dynamics and origin has been obtained from ground based observations of sodium D-line emissions. Since the discovery observation [Potter and Morgan, 1985], these emission lines have been the subject of observations by Potter and Morgan [1987, 1990, 1997a, 1997b], Potter *et al.* [1999, 2002], and Sprague *et al.* [1997, 1998]. Only two other elements of Mercury's exosphere have been identified from the Earth: potassium [Potter and Morgan, 1986; Sprague *et al.*, 1990; Sprague, 1992] and calcium [Bida *et al.*, 2000].

[3] The sodium observations at Mercury provide a principal test of the relative importance of the various proposed mechanisms leading to the formation of Mercury's exosphere and give guidance to our understanding of the formation of surface boundary-layer atmospheres on other solar system objects [Johnson, 2002]. Solar wind ion sputtering [Potter and Morgan, 1985], photon stimulated

desorption [McGrath et al., 1986] and thermal desorption [Hunten et al., 1988; Sprague, 1990, 1992, 1993; Hunten and Sprague, 1997, 2002; Sprague et al., 1997] were suggested to be important processes for producing Mercury's sodium exosphere with sputtering by impacting solar particles often quoted as the most likely explanation for the high latitude emission brightnesses observed at Mercury [Potter and Morgan, 1990, 1997a; Killen et al., 2001]. Micrometeoroid vaporization [Morgan et al., 1988] and chemically induced sputtering [Potter, 1995] were also suggested as a possible mechanisms for producing exospheric particles. Finally, the ejection and implantation of sodium by impacting magnetospheric ions have been discussed [e.g., Cheng et al., 1987; Sprague, 1992; Ip, 1993; Killen and Morgan, 1993; Killen and Sarantos, 2003; Delcourt et al., 2003], processes we evaluate here.

[4] There is no general agreement in these works about the relative importance of these processes of ejection. In particular, there is no agreement about the role of thermal desorption in the depletion of sodium in Mercury's surface [Sprague, 1990; Killen and Morgan, 1993] nor of the role of sodium ion implantation on the nightside, its subsequent diffusion inside Mercury's regolith and its release on exposure to sunlight [Sprague, 1992; Killen and Morgan, 1993]. Important studies of the sodium ejection processes have been carried out in the laboratory and have provided new information on the energy distribution and rate of ejection of sodium atoms from Lunar and Hermian type surfaces [Wiens et al., 1997; Madey et al., 1998; Yakshinskiy and Madey, 1999, 2000].

[5] In a previous paper [Leblanc and Johnson, 2003], we considered four processes thought to dominate the ejection of sodium from Mercury's surface and described their evolution with respect to Mercury's heliocentric position and to the location on Mercury's surface. The relative importance of each process and their potential competition in ejecting sodium atoms from Mercury's surface were taken into account and discussed in the context of the large set of observations of Mercury's sodium exosphere. The picture of the formation of Mercury's exosphere given by Leblanc and Johnson [2003] emphasizes the importance of the dayside depletion of sodium from the upper layers of surface material mainly induced by thermal desorption as predicted by Sprague [1990, 1992, 1993] and by Hunten and Sprague [1997, 2002]. This depletion reduces significantly the role of the solar wind sputtering in the formation of Mercury's sodium exosphere. The dayside to nightside migration of the sodium exospheric atoms was shown to be the origin of a local increase in the sodium concentration in Mercury's nightside surface at high latitudes. This leads to regions of enhanced ejection of sodium atoms on the dayside, producing sodium emission brightness peaks at high latitudes similar to the ones reported by Potter and Morgan [1990, 1997a].

[6] Due to desorption, transport and adsorption of returning sodium, the concentration of sodium in Mercury's upper surface was shown to be highly variable from dayside to nightside, from equatorial to polar latitudes and from Mercury's perihelion to Mercury's aphelion [Leblanc and Johnson, 2003]. One of the surprising consequence of Mercury's surface depletion is that the total content of sodium in Mercury's exosphere is larger at the aphelion

than at the perihelion. Indeed the Sun's rotation speed around Mercury changes from a maximum at the aphelion to a minimum at the perihelion [Sotter and Ulrichs, 1967]. This means that the speed with which the dawn terminator "moves" around Mercury changes with respect to Mercury's heliocentric position and that the rate with which surfaces that are replenished in sodium during Mercury's night reach Mercury's dayside varies as Mercury orbits the sun. In other words, the size of the sodium reservoir available for ejection into Mercury's exosphere is variable resulting in significant aphelion to perihelion variations of the sodium total content of Mercury's exosphere.

[7] Since the magnetospheric ion circulation was not properly treated by Leblanc and Johnson [2003], a realistic treatment is used here to examine the effect of re-impacting sodium ions. The model of Mercury's sodium exosphere is coupled to the model of ion circulation in Mercury's magnetosphere developed by Delcourt et al. [2002, 2003]. In section 2, we provide a brief description of our approach. In section 3 the characteristics of the magnetospheric ion bombardment of the surface are given, whereas in section 4 we discuss the potential role of the magnetospheric ion recycling on the formation of Mercury's neutral sodium exosphere formation. In section 5 we conclude.

2. Mercury's Sodium Exosphere and Magnetospheric Ion Circulation

[8] A detailed model for Mercury's neutral sodium exosphere was given by Leblanc and Johnson [2003]. It is a three-dimensional (3-D) model which describes the evolution of Mercury's sodium exosphere and the evolution of the sodium density in Mercury's upper surface during a full Mercury year. This approach takes into account diurnal and sidereal rotations and describes a self consistent system where loss and supply are intrinsically equilibrated averaged over one Mercury year. Our model is based on a Monte Carlo approach where the motion of test particles, each representing a large number of neutral sodium atoms, is followed ballistically. The test particles are produced by thermal and photon stimulated desorption, solar wind sputtering and micrometeoroid vaporization. The initial energy distributions are deduced from laboratory measurements: from Wiens et al. [1997] for solar wind sputtering, from Yakshinskiy and Madey [1999, 2000] for photon stimulated and thermal desorptions, and from Eichhorn [1978] for micrometeoroid vaporization. Rates of ejection and spatial distributions around Mercury are calculated taking into account gravity and solar radiation pressure forces. The trajectory of a test particle is calculated up to the moment when such particle is either ionized by solar photons, impacts the surface or escapes Mercury's gravitational attraction. Depletion and enrichment of Mercury's surface by ejection and reabsorption of these test particles are also calculated. Test particles are ejected from Mercury's surface with initial energy and spatial distributions associated with one of the four mechanisms of ejection. Thermal and photon-stimulated desorptions vary with longitude and latitude at Mercury's surface and with Mercury's distance to the Sun. These processes and ion sputtering also vary with the local Na concentration in Mercury's upper surface. Meteoroid bombardment is twice as intense on the leading face of

Mercury (the dawn side) than on the trailing face (the dusk side) [Killen and Ip, 1999]. As a first approximation, it is assumed to contribute an amount of sodium equal to the sodium content of the incident meteoroid flux, and therefore this supply rate does not depend on the surface concentration of Na atoms, nor does it change that concentration.

[9] Thermal and photon stimulated desorptions and solar wind sputtering act on the same Na atoms inside grains on the surface of Mercury's regolith. As a first approximation, these three processes of ejection are considered to be fully competitive with each other. We initially neglected replenishment of the surface concentration of sodium which can be induced by radiation-enhanced diffusion or mixing of the regolith [McGrath et al., 1986]. We also neglected the effect of surface charging and grain levitation and ignored the effect of a distribution in binding sites [Madey et al., 1998]. Solar wind sputtering is arbitrarily limited to the dayside, high latitude regions in agreement with Sarantos et al. [2001] and Massetti et al. [2003] even if nightside bombardment could also occur for particular interplanetary magnetic field orientation and strength [Kabin et al., 2000; Ip and Kopp, 2002; Kallio and Janhunen, 2003a, 2003b]. Photon stimulated desorption is proportional to the incident solar flux of photons with energy above 5 eV [Yakshinskiy and Madey, 1999]. The rate of ejection by thermal desorption from Mercury's surface materials increases quickly above a surface temperature equal to 350 K [Yakshinskiy et al., 2000].

[10] In the work of Leblanc and Johnson [2003], the exact trajectory of a newly ionized neutral Na exospheric atom was not calculated. A newly ionized particle was assumed either to be lost by Mercury if the ionization occurred above 10 km from Mercury's surface or to be reabsorbed by Mercury's surface if the ionization occurred below 10 km. In order to describe the ion circulation inside Mercury's magnetosphere, Delcourt et al. [2002, 2003] combined a model of Mercury's magnetosphere adapted from the Luhmann and Friesen [1979] model of the Earth magnetosphere with a model of the solar wind driven convection electric field deduced from Volland [1978] for the Earth's magnetosphere. This description of Mercury's magnetosphere and of Mercury's current system is based on the assumption that Mercury's magnetosphere can be approximated by a scaled version of the Earth's magnetosphere [Connerney and Ness, 1988; Luhmann et al., 1998]. Such an approach uses simple analytical models of Mercury's magnetosphere and current system which has the advantage of allowing fast computing.

[11] Test ion trajectories are computed by solving the equations of motion under the effect of electric and magnetic fields. Note that the full equation of motion is used because of the large field gradient encountered during transport [Delcourt et al., 2002]. The coupling between the neutral exospheric model [Leblanc and Johnson, 2003] and the ion exospheric model [Delcourt et al., 2003] is realized as follows: each time a test neutral is ionized, one test ion is created. Test ions and neutrals then move simultaneously on the same time scale. Test ions are considered as escaping Mercury's magnetosphere when they reach Mercury's magnetopause where they are dragged by the solar wind away from Mercury's gravitational field or when they reach more than four Mercury radii from

Mercury's center along the tail direction where they intersect the dusk magnetopause because of their large larmor radii [see Delcourt et al., 2003, Figure 10]. The third and last possibility is that test ions reimpact Mercury's surface where they sputter the surface and are implanted.

[12] Magnetospheric Na⁺ ions which reimpact Mercury's surface have energies between a few eV and a few tens of keV. The upper limit is constrained by the cross tail potential drop [Delcourt et al., 2003]. The steady state efficiency of such ions to sputter neutral Na atoms from Mercury's surface is here assumed to be equal to the sputtering rate of the surface silicate scaled by the sodium atom concentration [e.g., Johnson and Baragiola, 1991]. It will differ from that estimated for H⁺ and He²⁺ solar wind particles [Flavill et al., 1980; Killen et al., 2001]. The yield versus energy of the impacting ion, which is the total number of particles ejected from the surface per incident ion, is deduced from laboratory measurements. Such a yield is the sum of two contributions: the contribution due to ejection induced by nuclear elastic collisions in the surface layers and the contribution due to ejection induced by electronic excitation of the lattice [e.g., Johnson, 1990]. For the ejection efficiency induced by nuclear collisions, we scale the nuclear stopping power, $(dE/dx)_n$, which is the amount of energy lost by nuclear collisions in the surface per unit path length of the incident ion [Ziegler et al., 1985], to the measurements of the yield of Ar⁺ particles impacting SiO₂ surface [Betz and Wehner, 1983] and multiplied this by an appropriate mass factor [Andersen and Bay, 1981]. For the ejection induced by electronic excitation, we use the electronic stopping power $(dE/dx)_e$ [Ziegler et al., 1985], scaled to the yield of very energetic Cl⁺ particles impacting SiO₂ surface. These were then tested against a recent experiment for the sputtering of sodium intrinsic to or absorbed on a silicate (C. Dukes, personal communication, 2001). Consistent with that experiment, we assume there is no difference in binding, on the average, for intrinsic sodium atoms in a silicate and a sodium that has been reabsorbed and becomes bound to the silicate surface [Madey et al., 1998]. Using the values of $(dE/dx)_n$ and $(dE/dx)_e$ for Na⁺ particles impacting a SiO₂ surface vs energy [Ziegler et al., 1985], we combined the yields and deduced the yield vs energy of Na⁺ ion impacting SiO₂ surface in Figure 1. The crosses represent the yield vs energy induced by nuclear collision and the triangles the yield vs energy induced by electronic excitation. The sum of these two contributions is represented by the solid line. Flavill et al. [1980] reported laboratory measurements of a yield for He²⁺ impacting lunar type surface with typical solar wind energy (~3 keV) equal to 1/3 which is consistent with the yield indicated in Figure 1. We also performed calculations using TRIM software (Ziegler 1985) to simulate the bombardment of SiO₂ grains by Na⁺ particles and found very good agreement with Figure 1.

[13] Since surface porosity decreases the efficiency of ejection due to sticking on neighboring grains [Hapke and Cassidy, 1978; Johnson, 1989], a correction to the yield in Figure 1 is made in order to obtain the number of Na atoms ejected from Mercury's regolith per incident ion. In the work of Leblanc and Johnson [2003], the solar wind sputtering yield was reduced by a factor equal to 2.5 in order to recover the yield estimated by Johnson and

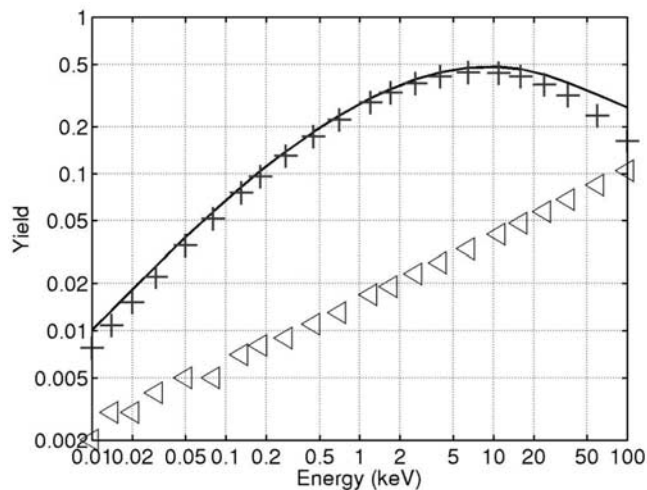


Figure 1. Total number of ejected particle per incident particle from a SiO_2 flat surface sputtered by Na type particle versus energy of the impactor (solid line). Total number of ejected particle per incident particle from a SiO_2 flat surface sputtered by Na type particle, due to nuclear collision (crosses) and due to electronic excitation of the lattice (triangles). The solid line is the sum of these two contributions.

Baragiola [1991] which is also the factor we used here. For the range of energy of the impacting Na^+ magnetospheric ion at Mercury's surface, that is from a few eVs up to a few of tens keV [*Delcourt et al.*, 2003], the ejection from the surface is dominated by ejection induced by nuclear collisions (Figure 1). The depth implantation of these Na^+ ion inside Mercury's surface has been estimated to be around 300 Å. The implanted sodium are typically lost in few Earth days by thermal desorption from the surface grains [*Sprague*, 1992; *Killen and Morgan*, 1993]. Here we simply include implantation as a local supply rate with the sodium removed by the ejection processes discussed before or by sputtering by re-impacting sodium ions.

[14] In our approach, each time that a test ion impacts the surface, a test neutral Na is ejected at the position of the impact. The weight of this test neutral is set equal to the product of the weight of the incident test ion times the yield of the test ion at the energy of the impactor (deduced from Figure 1) times the concentration of the surface in Na atoms. The initial velocity of the ejecta is calculated from a velocity distribution deduced from laboratory measurements [*Wiens et al.*, 1997] and is the same distribution as the one used for solar wind sputtering [*Leblanc and Johnson*, 2003]. To estimate its importance, magnetospheric ion sputtering is treated as an added process of ejection independent to the other processes. Such an assumption tends to slightly overestimate the rate of ejection induced by magnetospheric ion sputtering. Neutral atoms are permanently ejected from Mercury's surface and followed around Mercury within 50 Mercury radii (R_M) from Mercury's center during more than 6 Mercury's years. Each simulation starts from the exosphere and surface concentration displayed by *Leblanc and Johnson* [2003] at TAA = 125° . TAA is for True Anomaly Angle and corresponds to a particular heliocentric position of Mercury around the Sun. TAA = 0° is for

Mercury at perihelion and TAA = 180° for Mercury at aphelion. After 6 Mercury's years, a convergence of the simulation is reached; that is, no variation from one Mercury year to another in the results is observed. Therefore the results displayed in this paper correspond to the last Mercury year of each simulation.

3. Magnetospheric Ion Recycling

[15] Using the nominal conditions defined by *Delcourt et al.* [2003], that is a cross polar cap potential drop of 20 kV corresponding to normal solar wind conditions (solar wind speed of 400 km/s and an Interplanetary Magnetic Field (IMF) magnitude at Mercury equal to 30γ), we found that 15% of the magnetospheric Na^+ ions reimpact the surface. This percentage is close to the 10% of ions considered as reabsorbed by Mercury's surface that we found by using a simple approximation of the ion circulation of *Leblanc and Johnson* [2003]. As a consequence, the equilibrium between loss and supply reached by *Leblanc and Johnson* [2003] is not significantly changed by the use of the present ion circulation model. As a matter of fact, the agreement between *Potter et al.* [2002] measurements and *Leblanc and Johnson* [2003] simulation is found again here using the same total sodium supply rate to the surface, $3.5 \times 10^{23} \text{Na/s}$, as the one considered by *Leblanc and Johnson* [2003]. The 15% of magnetospheric Na^+ ions which reimpact the surface is an average over one Mercury year and has been calculated for steady state and average solar wind conditions (see also last paragraph of section 4). We do not describe here ion recycling due to solar field variability over very short time periods, the situation observed by *Potter et al.* [1999].

[16] Figure 2 displays the flux intensity (Figures 2a and 2c) and energy distributions (Figures 2b and 2d) of the Na^+ impacting particles. These fluxes have been obtained by averaging the flux of reimpacting magnetospheric ions between TAA = 124° and TAA = 181° (Figures 2c and 2d) and between TAA = 300° and TAA = 16° (Figures 2a and 2b) respectively. The values displayed Figure 2 are therefore the averaged flux and energy of the reimpacting magnetospheric ions on time scales of ~ 350 Earth hours (1/6 of one Mercury's year) and 300 Earth hours (1/7 of one Mercury's year) respectively. The flux of ions reimpacting Mercury's surface in Figure 2 can be divided into three parts:

[17] • The flux above $\pm 40^\circ$ in latitude is composed of low energy ions (Figures 2b and 2d). These are newly ionized neutrals which have been ejected from the surface at high latitudes. The ion densities displayed Figure 3 are obtained by integrating over 10 Earth hours around Mercury's position TAA = 16° for Figures 3a and 3b and around TAA = 181° for Figures 3c and 3d. Figures 3b and 3d display the ion density in a plane perpendicular to the equatorial plane at a longitude equal to -100° on the nightside (negative value for $(x^2 + y^2)^{1/2}$) and to 80° on the dayside (positive value of $(x^2 + y^2)^{1/2}$). This plane corresponds to the solid straight line plotted on Figures 3a and 3c. Only half of the plane perpendicular to the equatorial plane is shown since we assume symmetry between North and South hemispheres. In Figures 3b and 3d, peaks of ion density appear at high latitudes. These peaks correspond to the flux of reimpacting particles at high latitudes

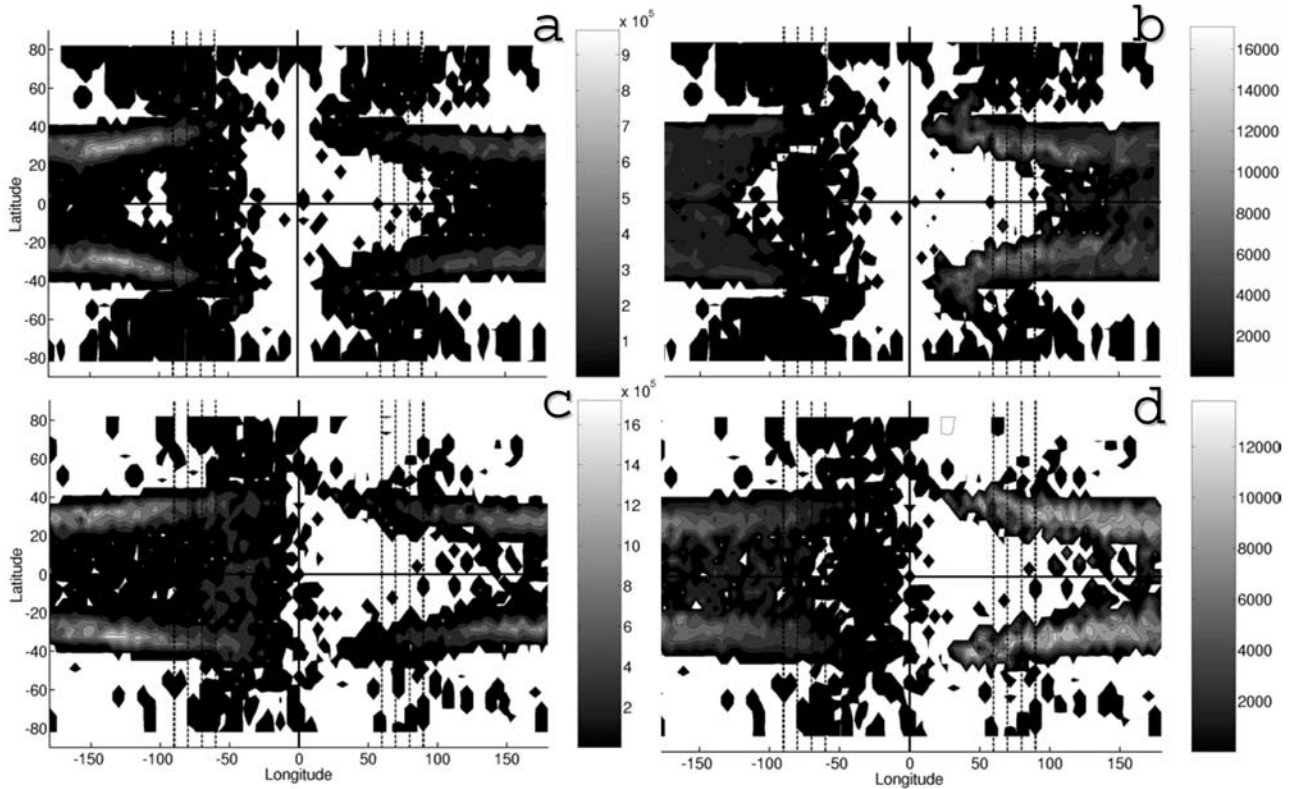


Figure 2. Flux (a and c) and energy (b and d) distributions of the magnetospheric Na^+ ion reimpacting Mercury's surface. These distributions are displayed at two positions around Mercury: (a and b) averaged between TAA = 300° and TAA = 16° and (c and d) averaged between TAA = 124° and TAA = 181° . Flux are in $\text{Na}^+/\text{cm}^2/\text{s}$ and energy in eV. Mercury subsolar point is at the center of each panel, the horizontal line represents the equator line, and the vertical line the subsolar line. Dayside is between $\pm 90^\circ$ in longitude (thickest dashed vertical lines). Thin vertical dashed lines at $\pm 80^\circ$, $\pm 70^\circ$, and $\pm 60^\circ$ in longitude are also plotted. The white areas (as an example at the center of Figure 2a) correspond to area with flux of impacting particles lower than $5 \times 10^4 \text{ Na}^+/\text{cm}^2/\text{s}$ (a and b) and than $10^5 \text{ Na}^+/\text{cm}^2/\text{s}$ (c and d).

displayed in Figure 2. They also appear to correlate spatially to peaks of neutral density as shown in Figure 4 which has been obtained with the same averaging as for Figure 3. As explained by *Ip* [1990], such peaks in the neutral density are induced by the solar radiation pressure.

[18] • In Figure 2, the flux concentrated between $\pm 20^\circ$, 40° in latitude are composed of the most energetic ions (Figures 2b and 2d). These reimpact on the dusk side of the planet (above $+50^\circ$ in longitude) and on the nightside (Figures 2a and 2c). As demonstrated by *Delcourt et al.* [2003], this downward flux corresponds to ions that have circulated in the nightside plasma sheath and experienced non-adiabatic intersection with the neutral sheath. These fluxes resemble auroral precipitation at Earth. However, the poleward boundary here does not coincide with the open flux region but with the limit of the non-adiabatic motion in the mid tail. They represent the largest fraction of the magnetospheric ions that reimpact Mercury's surface. *Delcourt et al.* [2003, 2003] used a model for the Na neutral exosphere determined by an ejection rate that peaks at the subsolar point and is symmetric about the subsolar line. This model is significantly different from the one of *Leblanc and Johnson* [2003]. However the same high latitude bands of reimpacting magnetospheric ion were

found in both works. Therefore the results for this component do not appear to be significantly affected by the near surface model of neutral exosphere but depend on the availability of Na at high altitudes and on the model of Mercury's magnetosphere being like that of the Earth. Actually, *Kallio and Janhunen* [2003a, 2003b] have recently published the results of a 3-D hybrid magnetosphere approach showing the impact of the solar wind particles at Mercury's surface for different IMF conditions. These authors also found high latitude bands of solar wind ion impact around $\pm 30^\circ$ for all the different IMF conditions they considered [*Kallio and Janhunen*, 2003b].

[19] • Another component of the flux of Na^+ reimpacting Mercury's surface is equatorial and is mainly concentrated on the nightside in Figures 2a and 2b between $[-180^\circ, -40^\circ]$ and $[100^\circ, 180^\circ]$ and in Figures 2c and 2d between $[-180^\circ, 0^\circ]$ in longitude. This is a contribution which does not appear in the work of *Delcourt et al.* [2003]. It is due to the use of a different neutral exosphere in this paper. Such a flux is mainly composed of particles with energy between 1 to 4 keV which remain close to the dawn flank of Mercury's magnetosphere before impacting the surface. This is true in particular in Figures 2c and 2d and is produced by the peak in the neutral density between longitudes $[-180^\circ, 0^\circ]$ as

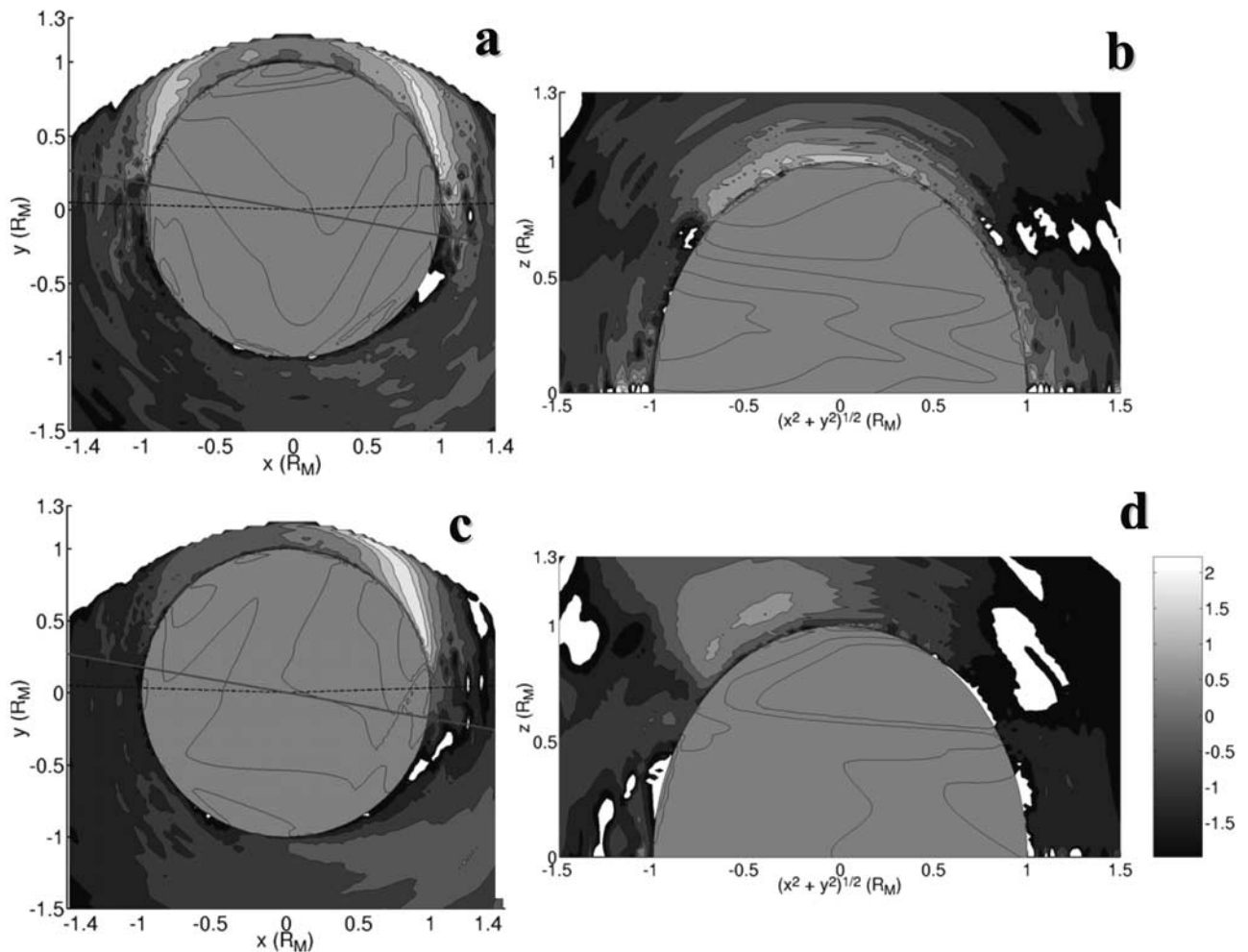


Figure 3. Ion density (Log_{10} of Na^+/cm^3) inside Mercury's magnetosphere integrated at two positions of Mercury around the Sun: TAA = 16° (a and b) and TAA = 181° (c and d). These densities are averaged of the density during 10 Earth hours around the indicated Mercury's position. Figures 3a and 3c display the ion density in the equatorial plane and Figures 3b and 3d the ion density in a plane perpendicular to the equatorial plane with the North and South poles. The intersection of this plane with the equatorial plane is indicated by the solid straight line in the left panels. The Sun in Figures 3a and 3c is in the direction of the y positive. In Figures 3b and 3d, the positive $(x^2 + y^2)^{1/2}$ part of the axis corresponds to the part of the straight solid line in Figures 3a and 3c within $y > 0$ (the dayside hemisphere) and the negative $(x^2 + y^2)^{1/2}$ part of the axis to $y < 0$ (the nightside hemisphere). The white areas (as an example at the left upper corner of Figure 3b) correspond to area with density lower than $10^{-2} \text{ Na}^+/\text{cm}^3$.

shown in Figure 4c (at $X \sim R_M$ and $Y \sim 0.25 R_M$). In the model of neutral exosphere used by *Delcourt et al.* [2003] the sodium density peaked at the subsolar point. The difference between the reimpacting fluxes in the equatorial regions displayed Figures 2a and 2b, is due to the difference in the distribution of the ion density around Mercury (Figures 3a and 3c) in particular to a significant peak of ion density on the dusk side of Mercury at TAA = 16° (Figure 3a) which does not appear at TAA = 181° (Figure 3c).

[20] The density distribution of the Na^+ ion around Mercury displayed in Figure 3 is derived from the density distribution of the Na atoms which is displayed in Figure 4. The large peak of ion density on the dawn side (Figures 3a and 3c at $X \sim 1 R_M$ and $Y \sim 0.5 R_M$) is due to the peak in the atmospheric density which is generated by a peak in the ejection rate from the surface (Figures 4a and 4c). A second

peak in the ion density occurs at TAA = 16° (Figure 3a, $X \sim -1 R_M$ and $Y \sim 0.5 R_M$). It is due to a peak in the neutral density, like that shown in Figure 4a, which is induced by the particular Sun and Mercury rotation velocities at this Mercury's heliocentric position [*Leblanc and Johnson, 2003*]. The region of high ion density in Figures 3a and 3c is significantly elongated toward the dayside magnetopause (the limit of the plot at positive Y values). At dayside equatorial latitudes, ions move toward the Sun because of the sunward motion of Mercury's magnetospheric field lines at low magnetic latitudes. Maxima of the ion density are equal to ~ 10 and $\sim 100 \text{ Na}^+/\text{cm}^3$ at TAA = 16° and TAA = 181° respectively and occur roughly 0° and 20° in longitude after the dawn terminator respectively. The differences in the neutral density distributions at the two TAA in Figure 4 are mainly due to differences in the surface temperatures. At

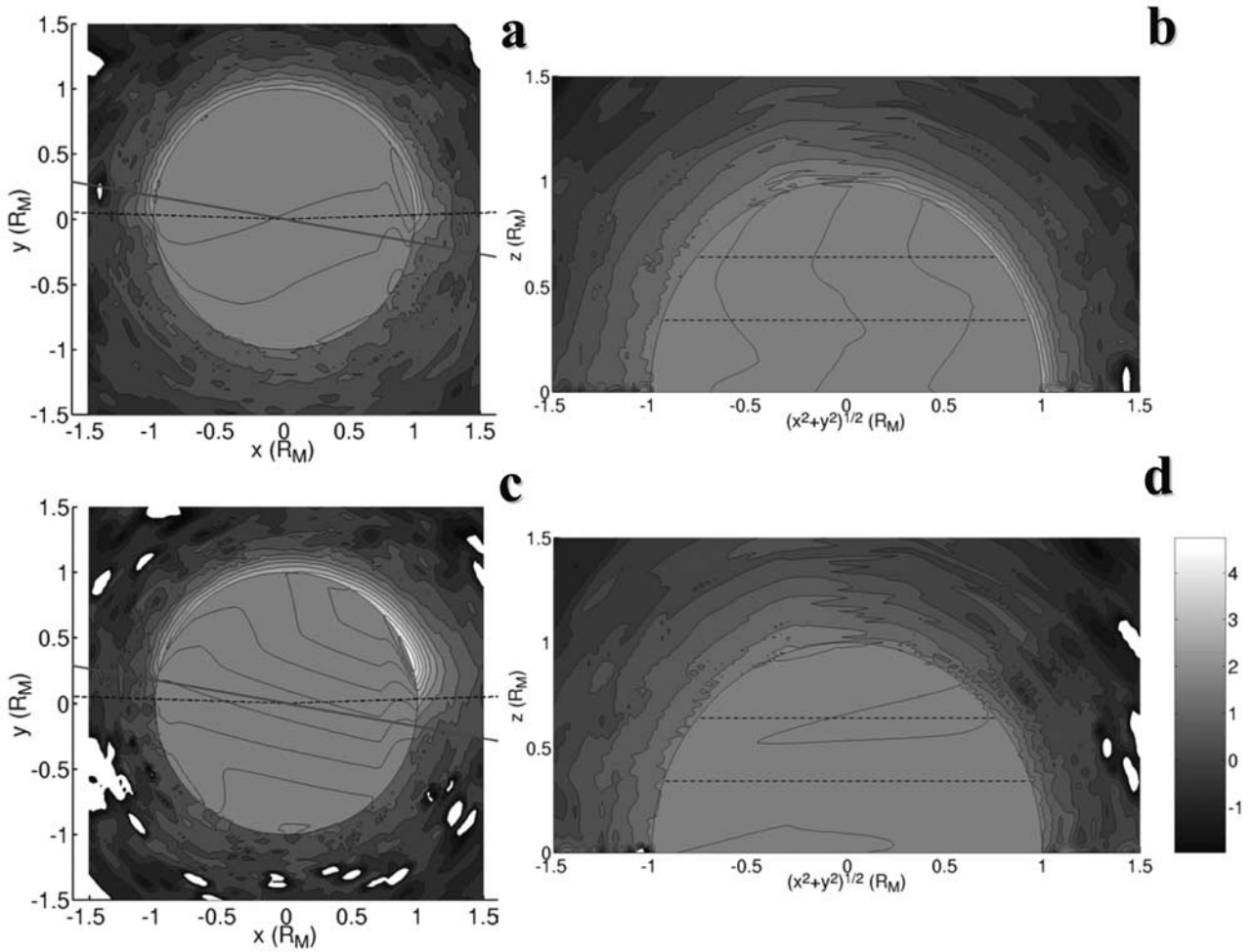


Figure 4. Neutral density (Log_{10} of Na/cm^3). Same legend as Figure 3.

TAA = 16° , the surface temperature is larger close to the terminators than at TAA = 181° and as a consequence neutral particles are ejected from Mercury's surface closer to the terminators at TAA = 16° than at TAA = 181° . Figure 4 shows also that there is no apparent increase in the neutral density close to the surface bombarded by the magnetospheric ions (between the two horizontal dashed lines which correspond to latitude $+20^\circ$ and $+40^\circ$) in the plane perpendicular to the equatorial plane (Figures 4b and 4d). This plane was suggested as one of the regions where the magnetospheric ion sputtering might be the largest (Figure 2).

[21] Maxima of the Na neutral density close to the surface are equal to $5 \times 10^4 \text{ Na}/\text{cm}^3$ at the aphelion and to $10^3 \text{ Na}/\text{cm}^3$ at the perihelion. At 400 km from the surface, such maxima of the neutral density decrease down to $200 \text{ Na}/\text{cm}^3$ at the aphelion and down to $30 \text{ Na}/\text{cm}^3$ at the perihelion.

4. Consequences for Mercury's Neutral Na Exosphere

[22] The bombardment of the surface by recycled sodium ions has two main consequences for Mercury's neutral sodium exosphere:

[23] • ejection of new neutral Na atoms by sputtering which reduces the sodium concentration in the surface and increases the population of the exosphere,

[24] • implantation of sodium into Mercury's surface layers leading to an increase of the sodium concentration in the surface.

[25] The sodium ejection rate by the reimpacting magnetospheric ions is much smaller than the ejection rates for the other processes of ejection. It is maximum around the aphelion and minimum around the perihelion because the neutral exosphere and therefore the ion exosphere are much less dense at the perihelion than at the aphelion (Figures 3 and 4). The total number of ejecta per second due to magnetospheric ion sputtering is always two orders of magnitude smaller than the number of ejecta per second due to solar wind sputtering and three orders of magnitude less than photon stimulated desorption and micrometeoroid vaporization. The total number of Na^+ reimpacting the surface is $\sim 5 \times 10^{22} \text{ Na}^+/\text{s}$ averaged over one Mercury year, varying from $\sim 2 \times 10^{23}$ to $\sim 2 \times 10^{21} \text{ Na}^+/\text{s}$ from aphelion to TAA = 75° where it is minimum. The average efficiency of these ions for ejecting sodium is less than 0.01. This can be deduced from Figure 1 corrected by the average concentration of Na atoms inside Mercury's upper surface (between 0.003 and 0.01) and corrected by the porosity reduction factor (2.5). Therefore, even if all the new magnetospheric ion reimpact Mercury's surface (that is, around $\sim 4 \times 10^{23} \text{ Na}^+/\text{s}$), this sputtering effect is much smaller than the other ejection processes. Magnetospheric ion sputtering

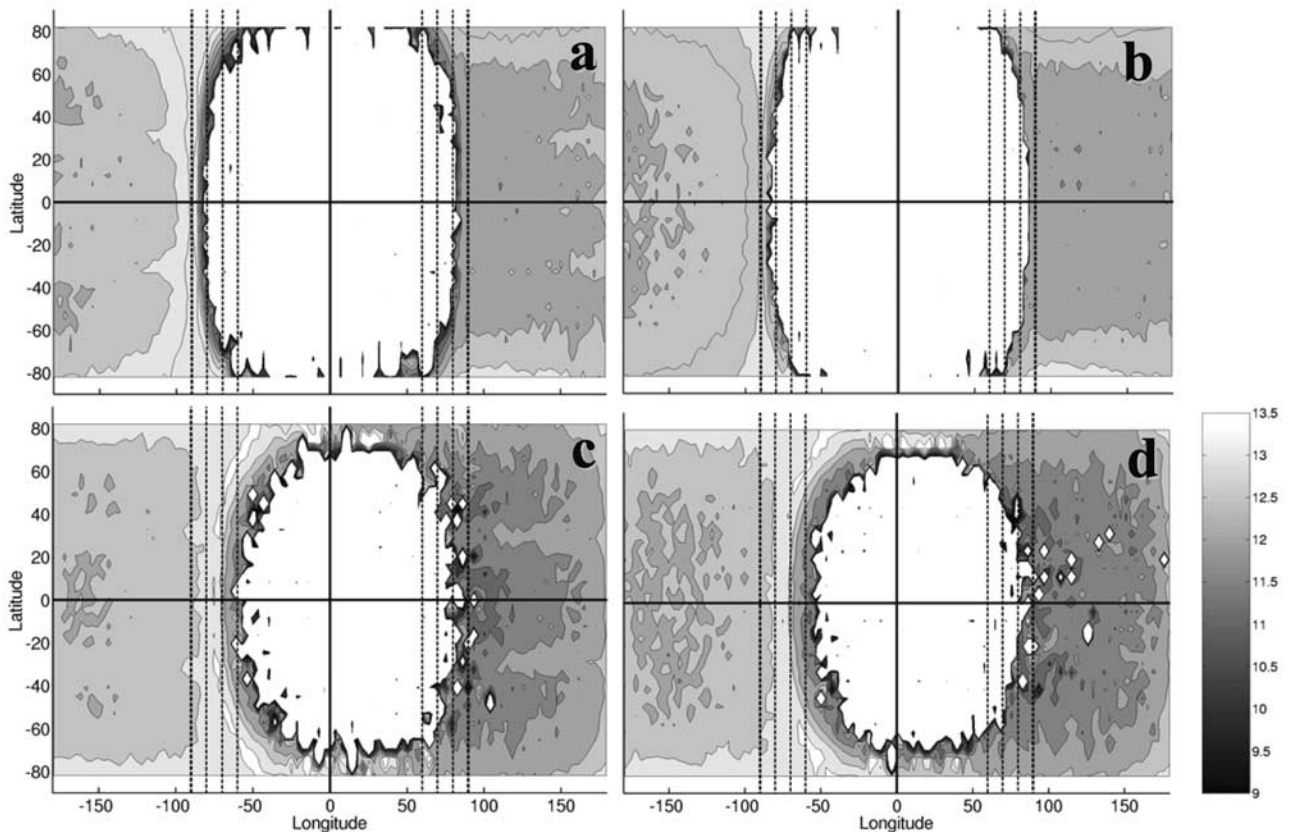


Figure 5. Surface density distribution (Log_{10} of Na/cm^2) calculated at TAA = 16° (a and b) and at TAA = 181° (c and d). Mercury subsolar point is at the center of each panel, the dark horizontal line represents the equator line, and the dark vertical line the subsolar line. Dayside is between $\pm 90^\circ$ in longitude (thickest dashed vertical lines). Thin vertical dashed lines at $\pm 80^\circ$, $\pm 70^\circ$, and $\pm 60^\circ$ in longitude are also plotted. Scale bar for the four panels is indicated at the right bottom. Left column: present model. Right column: *Leblanc and Johnson* [2003] model. The white areas (at the center of each panel) correspond to area with surface density lower than $10^9 \text{ Na}/\text{cm}^2$.

could be important if there exists a significant exospheric component of some other species such as oxygen.

[26] Because the flux of reimpacting magnetospheric Na^+ is highly localized (see Figure 2), local peaks of ejection induced by Na^+ magnetospheric ion sputtering are possible. These peaks would only be observable in very narrow regions between latitudes $\pm[20^\circ, 40^\circ]$ as suggested by Figure 2 and in particular on Mercury's nightside where other processes of ejection do not act. However, they do not stand out on the grid used in the model calculations (e.g., Figure 4).

[27] The implantation of the largest fraction of the Na^+ ions reimpacting the surface increased the density of Na in Mercury's surface. Figure 5 provides the Na density in Mercury's surface as obtained with the present model for a potential cross polar drop of 20 kV (Figures 5a and 5c) and as obtained with the model used by *Leblanc and Johnson* [2003] (Figures 5b and 5d). We display the distribution of Mercury's surface density near perihelion (TAA = 16° , Figures 5a and 5b) and near aphelion (TAA = 181° , Figures 5c and 5d).

[28] The increase of the Na density in Mercury's upper surface around $\pm 30^\circ$ latitude is obvious at both TAA and is clearly related to the flux of magnetospheric ions reim-

pacting Mercury's surface (Figure 2). Such increase appears earlier at TAA = 181° (in term of longitude) than at TAA = 16° because of the larger flux of ion reimpacting Mercury's surface at TAA = 181° (Figures 2a and 2b).

[29] A consequence of this increase in the Na density is a local enhancement of the ejection rate of Na atoms when these regions reach Mercury's dayside. This effect has been suggested by *Sprague* [1992a], who calculated that diffusion from implantation depth of these reimpacting Na^+ (300 \AA) up to the surface could produce peaks of ejection in the exosphere far from the dawn terminator close to noon longitude in agreement with observations. This point was criticized by *Killen and Morgan* [1993], who argued that such diffusion was actually much faster than calculated by *Sprague* [1992] and therefore should only produce narrow peaks of ejection at the dawn terminator which could not be related to observations. In this paper we consider that any implanted Na^+ will be ejected from the surface as fast as reabsorbed neutral Na atoms which do not penetrate deeply in upper surface grains. In Figure 6, we plotted the column density seen at a phase angle of 50° and TAA = 181° calculated using the present model, Figure 6a and for TAA = 300° at a phase angle of 120° in Figure 6c. In Figures 6b and 6d, we plotted the column density displayed in

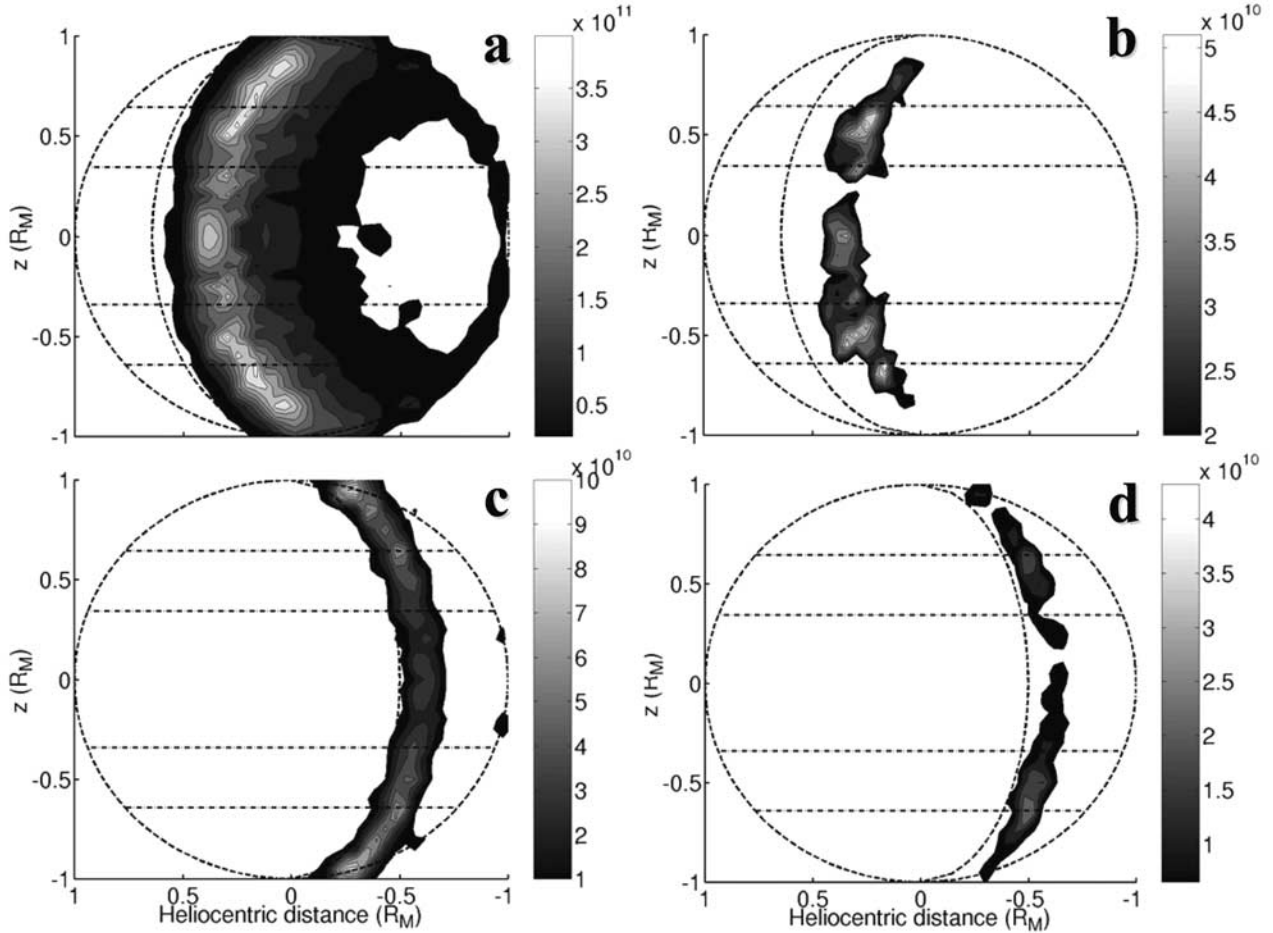


Figure 6. Left column: sodium column density (Na/cm^2) obtained with the present model. Right column: results of the left column minus the results obtained without ion circulation model [Leblanc and Johnson, 2003] in Na/cm^2 . (a and b) At TAA = 181° as seen for a phase angle of 50° (angle between the Earth/Mercury and the Sun/Mercury directions). (c and d) At TAA = 300° with a phase angle of 120° . +Z value corresponds to the North pole. Dashed circle line represents the limit of Mercury surface and the dashed vertical line inside each circle the terminator at such phase angle. The Sun is placed at the right side (negative heliocentric distances). The four horizontal dashed lines correspond from top to bottom lines to latitude of 40° , 20° , -20° and -40° respectively. The white areas (as an example at the center of Figure 6c) correspond to area with sodium column density lower than the low limit of the scale bar.

Figures 6a and 6c minus the corresponding column density for same TAA and phase angle obtained by Leblanc and Johnson [2003], that is, without an ion circulation model. Figures 6b and 6d show that a significant local increase of the column density (see scale bars of Figures 6a and 6b and scale bars of Figures 6c and 6d) is associated with the increase of the surface density between $\pm[20^\circ, 40^\circ]$. Such an increase represents around 30% of the column density at these latitudes near the aphelion and around 60% near the perihelion. It also induces local maxima that can be of the same order or even greater than the maxima of the column density usually observed at higher latitudes. Therefore implantation of magnetospheric Na^+ can contribute to the observed maxima in Na emission brightness and observation of the peaks in the exospheric emissions at high latitudes by ground based UV instruments [Potter and Morgan, 1990]. Therefore such observations can indicate whether or not Mercury's magnetosphere is similar to Earth's.

[30] The intensity of the cross-polar cap potential drop in the Delcourt *et al.* [2003] model is directly related to the solar wind velocity. We also considered two other cases of cross polar potential drop: one of 10 kV (corresponding to slow solar wind condition with a velocity of 200 km/s) and the other of 35 kV (a fast solar wind condition with velocity of 750 km/s). Starting from the same initial conditions at TAA = 230° , we simulate 2 Earth hours and integrated the results during the last 1/2 Earth hour. Such simulations can track possible variations in Mercury's exosphere under varying solar wind velocities. However, significant variations in Mercury's neutral exosphere were not seen due the changes in Na^+ ion energies and fluxes. The energy range of the reimpacting particle is different in the three cases, with the largest potential drop leading to the greatest acceleration. In going from the smallest to the largest potential drop, the increased ion energies result in an increased sputtering yield but also to a factor of 2 to 3 decrease in the ion density. This occurs because the larger potential drop leads

to a shorter residence time of an ion inside Mercury's magnetosphere.

[31] The choice of the model of Mercury's magnetosphere [Luhmann and Friesen, 1979] does not allow for variations in the overall magnetospheric structure. In particular it can not account for changes induced by the IMF orientation. The IMF orientation and strength can significantly affect the proportion of open magnetic field lines if the assumption of an Earth-like magnetosphere is correct [Luhmann et al., 1998]. Variations in the proportion of open field lines can lead to significant variations of the number of ion trapped inside Mercury's magnetosphere [Leblanc et al., 2003] and more extended precipitation regions. This in turn can lead to significant variations of the rate of reimpact of magnetospheric ions into Mercury's surface as well as significant variations in precipitating solar ions [Killen and Sarantos, 2003]. As shown in Figure 6, with only 15% of the magnetospheric ions reimpacting Mercury's surface an observable effect is produced in the column density as seen from the Earth. Therefore a larger percentage of reimpacting ions, which might be associated, for example, with a particularly long period of positive Bz IMF [Luhmann et al., 1998], could lead to stronger short term increases in the Na column density than the average values calculated in this paper.

5. Conclusion

[32] This paper is the first attempt to dynamically couple a full Monte Carlo model of the formation of Mercury's sodium exosphere [Leblanc and Johnson, 2003] with a model of Na⁺ ion circulation at Mercury [Delcourt et al., 2003]. The circulation model is based on the assumption that Mercury's magnetosphere is a reduced model of the Earth's [Connerney and Ness, 1988]. The coupled calculations allow us to self consistently treat a system composed of Mercury's sodium exosphere, the surface concentration of sodium, and the recycling of the sodium magnetospheric ions.

[33] When the loss and supply of Na atoms at Mercury over one Mercury year are balanced, it is found that the recycling of magnetospheric Na⁺ ions to Mercury's surface remains small (less than 15% of the total number of new magnetospheric Na⁺ ion created). This result does not depend significantly on the cross-polar cap potential drop. The sputtering effect induced by sodium magnetospheric ions reimpacting Mercury's surface is small relative to solar wind sputtering because of the small flux of magnetospheric ions reimpacting Mercury's surface. Because the sputtering yield is also small, the number of Na⁺ magnetospheric ion reabsorbed in Mercury's upper surface is larger than the number of Na atoms ejected by the Na⁺ ions. As a consequence, the Na⁺ flux can locally enhance the Na density in the surface over the long Mercury night. This is particularly the case in narrow bands of latitudes directly defined by the structure of Mercury's magnetosphere. When such regions of enhanced sodium density reach Mercury's dayside, the sodium is rapidly depleted by thermal and photon-induced desorption and a local increase in the Na exospheric column density can be observed in Mercury's morning side exosphere. Such an effect could be the origin of some of the low latitude peaks of sodium D line emission

brightness observed at Mercury [Potter and Morgan, 1990, 1997a; Potter et al., 1999].

[34] In this paper we used the model of Mercury's exosphere by Leblanc and Johnson [2003] in which new sodium was supplied to Mercury's surface only by micro-meteorite impact. In the work of Leblanc and Johnson [2003] other supply rates (diffusion, mixing, etc.) were also considered. However, their effect on the atmospheric structure, though not negligible, would not significantly modify the results for ion recycling calculated here.

[35] Being able to describe the effect on the sodium atmosphere due to the coupling with the magnetosphere could eventually be a way of remotely monitoring the behavior of Mercury's magnetosphere. Variations in the flux of recycled magnetospheric ions induced by variable solar wind conditions (solar wind velocity or IMF orientation) can contribute to the short time variations seen in the sodium exospheric emissions. Treating this effect of the exosphere/magnetosphere coupling would require that we replace the present model of Mercury's magnetosphere [Delcourt et al., 2002, 2003] with a magnetospheric model like the one described by Luhmann et al. [1998]. Although larger short-term enhancements than those calculated here due to temporal changes in the IMF [Luhmann et al., 1998] might be expected, here we calculated the average enhancement in the exosphere due to ion recycling. We found that the size of this effect is consistent with the estimate given by Leblanc and Johnson [2003] and therefore does not significantly change the picture of Mercury's sodium atmosphere developed in that paper.

[36] **Acknowledgments.** The work at Virginia is supported by NASA's Planetary Atmospheres Program and Planetary Geology and Geophysics Program. We thank M. Liu for providing results of calculations used to generate Figure 1.

References

- Andersen, H. H., and H. L. Bay, Sputtering yield measurements, in *Berisch R(ed) Sputtering by Particle Bombardment*, pp. 145–218, Springer-Verlag, New York, 1981.
- Bida, T. A., R. M. Killen, and T. H. Morgan, Discovery of calcium in Mercury's atmosphere, *Nature*, 404, 159–161, 2000.
- Betz, G., and G. K. Wehner, Sputtering of multicomponent materials, in *Berisch R(ed) Sputtering by Particle Bombardment II*, pp. 11–90, Springer-Verlag, New York, 1983.
- Broadfoot, A. L., D. E. Shemansky, and S. Kumar, Mariner 10: Mercury atmosphere, *Geophys. Res. Lett.*, 3, 577–580, 1976.
- Cheng, A. F., R. E. Johnson, S. M. Krimigis, and L. J. Lanzerotti, Magnetosphere, exosphere and surface of Mercury, *Icarus*, 71, 430–440, 1987.
- Connerney, J. E. P., and N. F. Ness, Mercury's magnetic field and interior, in *Mercury*, edited by F. Vilas, C. R. Chapman, and M. S. Matthews, pp. 494–513, Univ. of Ariz. Press, Tucson, 1988.
- Delcourt, D. C., T. E. Moore, S. Orsini, A. Millilo, and J.-A. Sauvaud, Centrifugal acceleration of ions near Mercury, *Geophys. Res. Lett.*, 29(12), 1591, doi:10.1029/2001GL013829, 2002.
- Delcourt, D. C., S. Grimald, F. Leblanc, J.-J. Bertherlier, A. Millilo, and A. Mura, A quantitative model of planetary Na⁺ contribution to Mercury's magnetosphere, *Ann. Geophys.*, 21, 1723–1736, 2003.
- Eichhorn, G., Heating and vaporization during hypervelocity particle impact, *Planet. Space Sci.*, 26, 463–467, 1978.
- Flavill, R. P., W. C. Carey, M. McDonnell, D. G. Ashworth, and R. J. Allison, Progress in defining the solar wind sputter rate on protoplanets and interplanetary matter, *Planet. Space Sci.*, 28, 511–524, 1980.
- Hapke, B. W., and W. A. Cassidy, Is the Moon really as smooth as a billiard ball? Remarks concerning recent models of sputtering on the lunar surface, *Geophys. Res. Lett.*, 5, 297–300, 1978.
- Hunten, D. M., and A. L. Sprague, Origin and character of the lunar and Mercurian atmospheres, *Adv. Space Res.*, 19, 1191–1195, 1997.
- Hunten, D. M., and A. L. Sprague, Diurnal variation of Na and K at Mercury, *Meteorit. Planet. Sci.*, 37, 1165, 2002.

- Hunten, D. M., T. H. Morgan, and D. E. Shemansky, The Mercury atmosphere, in *Mercury*, edited by F. Vilas, C. R. Chapman, and M. S. Matthews, pp. 562–612, Univ. of Ariz. Press, Tucson, 1988.
- Ip, W.-H., On solar radiation-driven surface transport of sodium atoms at Mercury, *Astrophys. J.*, *365*, 675–681, 1990.
- Ip, W.-H., On the surface sputtering effects of magnetospheric charged particles at Mercury, *Astrophys. J.*, *418*, 451–456, 1993.
- Ip, W.-H., and A. Kopp, MHD simulations of the solar wind interaction with Mercury, *J. Geophys. Res.*, *107*(A11), 1348, doi:10.1029/2001JA009171, 2002.
- Johnson, R. E., Application of laboratory data to the sputtering of a planetary regolith, *Icarus*, *78*, 206–210, 1989.
- Johnson, R. E., *Energetic Charged-Particle Interactions With Atmospheres and Surfaces*, Springer-Verlag, New York, 1990.
- Johnson, R. E., Surface boundary layer atmospheres, in *Atmospheres in the Solar System: Comparative Aeronomy*, *Geophys. Monogr. Ser.*, vol. 130, pp. 203–219, AGU, Washington, D. C., 2002.
- Johnson, R. E., and R. A. Baragiola, Lunar surface: Sputtering and secondary ion mass spectrometry, *Geophys. Res. Lett.*, *18*, 2169–2178, 1991.
- Kabin, K., T. I. Gombosi, D. L. DeZeeuw, and K. G. Powell, Interaction of Mercury with the solar wind, *Icarus*, *143*, 397–406, 2000.
- Kallio, E., and P. Janhunen, Modelling the solar wind interaction with Mercury by a quasineutral hybrid model, *Ann. Geophys.*, in press, 2003a.
- Kallio, E., and P. Janhunen, Solar wind and magnetospheric ion impact on Mercury's surface, *Geophys. Res. Lett.*, *30*(17), 1877, doi:10.1029/2003GL017842, 2003b.
- Killen, R. M., and W.-H. Ip, The surface bounded atmospheres of Mercury and the Moon, *Rev. Geophys.*, *37*, 361–406, 1999.
- Killen, R. M., and T. H. Morgan, Diffusion of Na and K in the uppermost regolith of Mercury, *J. Geophys. Res.*, *98*, 23,589–23,601, 1993.
- Killen, R. M., and M. Sarantos, Space weather at Mercury, *Adv. Space Res.*, in press, 2003.
- Killen, R. M., A. E. Potter, P. Reiff, M. Sarantos, B. V. Jackson, P. Hick, and B. Giles, Evidence for space weather at Mercury, *J. Geophys. Res.*, *106*, 20,509–20,525, 2001.
- Leblanc, F., and R. E. Johnson, Mercury sodium exosphere, *Icarus*, *164*, 261–281, 2003.
- Leblanc, F., J. G. Luhmann, R. E. Johnson, and M. Liu, Solar energetic particle event at Mercury, *Planet. Space Sci.*, *51*, 339–352, 2003.
- Luhmann, J. G., and L. M. Friesen, A simple model of the magnetosphere, *J. Geophys. Res.*, *84*, 4405–4408, 1979.
- Luhmann, J. G., C. T. Russell, and N. A. Tsyganenko, Disturbances in Mercury's magnetosphere: Are the Mariner 10 "substorms" simply driven?, *J. Geophys. Res.*, *103*, 9113–9119, 1998.
- Madey, T. E., B. V. Yakshinskiy, V. N. Ageev, and R. E. Johnson, Desorption of alkali atoms and ions from oxide surfaces: Relevance to origins of Na and K in atmospheres of Mercury and the Moon, *J. Geophys. Res.*, *103*, 5873–5887, 1998.
- Massetti, S., S. Orsini, A. Milillo, A. Mura, E. De Angelis, H. Lammer, and P. Wurz, Mapping of the cusp plasma precipitation on the surface of Mercury, *Icarus*, in press, 2003.
- McGrath, M. A., R. E. Johnson, and L. J. Lanzerotti, Sputtering of sodium on the planet Mercury, *Nature*, *323*, 694–696, 1986.
- Morgan, T. H., H. A. Zook, and A. E. Potter, Impact-driven supply of sodium and potassium to the atmosphere of Mercury, *Icarus*, *75*, 156–170, 1988.
- Ness, N. F., K. W. Behannon, R. P. Lepping, Y. C. Whang, and K. H. Shatten, Magnetic field observations near Mercury: Preliminary results from Mariner 10, *Science*, *185*, 151–160, 1974.
- Potter, A. E., Chemical sputtering could produce sodium vapor and ice on Mercury, *Geophys. Res. Lett.*, *22*, 3289–3292, 1995.
- Potter, A. E., and T. H. Morgan, Discovery of sodium in the atmosphere of Mercury, *Science*, *229*, 651–653, 1985.
- Potter, A. E., and T. H. Morgan, Potassium in the atmosphere of Mercury, *Icarus*, *67*, 336–340, 1986.
- Potter, A. E., and T. H. Morgan, Variation of sodium on Mercury with solar radiation pressure, *Icarus*, *71*, 472–477, 1987.
- Potter, A. E., and T. H. Morgan, Evidence for magnetospheric effects on the sodium atmosphere of Mercury, *Science*, *248*, 835–838, 1990.
- Potter, A. E., and T. H. Morgan, Evidence for suprathreshold sodium on Mercury, *Adv. Space Res.*, *19*, 1571–1576, 1997a.
- Potter, A. E., and T. H. Morgan, Sodium and potassium atmospheres of Mercury, *Planet. Space Sci.*, *45*, 95–100, 1997b.
- Potter, A. E., T. H. Morgan, and R. M. Killen, Rapid changes in the sodium exosphere of Mercury, *Planet. Space Sci.*, *47*, 1441–1449, 1999.
- Potter, A. E., R. M. Killen, and T. H. Morgan, The sodium tail of Mercury, *Meteorit. Planet. Sci.*, *37*, 1165–1172, 2002.
- Sarantos, M., P. H. Reiff, T. W. Hill, R. M. Killen, and A. L. Urquhart, A bx-interconnected magnetosphere model for Mercury, *Planet. Space Sci.*, *49*, 1629–1635, 2001.
- Sotter, S., and J. Ulrichs, Rotation and heating of the planet Mercury, *Nature*, *214*, 1315–1316, 1967.
- Sprague, A. L., A diffusion source for sodium and potassium in the atmospheres of Mercury and the Moon, *Icarus*, *84*, 93–105, 1990.
- Sprague, A. L., Mercury's atmospheric sodium bright spots and potassium variations: A possible cause, *J. Geophys. Res.*, *97*, 18,257–18,264, 1992.
- Sprague, A. L., Correction to "Mercury's atmospheric sodium bright spots and potassium variations: A possible cause," *J. Geophys. Res.*, *98*, 1231, 1993.
- Sprague, A. L., R. W. H. Kozlowski, and D. M. Hunten, Caloris Basin: An enhanced source for potassium in Mercury's atmosphere, *Science*, *249*, 1140–1143, 1990.
- Sprague, A. L., R. W. H. Kozlowski, and D. M. Hunten, Distribution and abundance of sodium in Mercury's atmosphere, 1985–1988, *Icarus*, *129*, 506–527, 1997.
- Sprague, A. L., W. J. Schmitt, and R. E. Hill, Mercury: Sodium atmospheric enhancements, radar bright spots, and visible surface features, *Icarus*, *135*, 60–68, 1998.
- Volland, H., A model of the magnetospheric convection electric field, *J. Geophys. Res.*, *83*, 2695–2699, 1978.
- Wiens, R. C., D. S. Burnett, W. F. Calaway, C. S. Hansen, K. R. Lykkem, and M. L. Pellin, Sputtering products of sodium sulfate: Implications for Io's surface and for sodium bearing molecules in the Io torus, *Icarus*, *128*, 386–397, 1997.
- Yakshinskiy, B. V., and T. E. Madey, Photon-stimulated desorption as a substantial source of sodium in the lunar atmosphere, *Nature*, *400*, 642–644, 1999.
- Yakshinskiy, B. V., T. E. Madey, and V. N. Ageev, Thermal desorption of sodium atoms from thin SiO₂ films, *Surface Rev. Lett.*, *7*, 75–87, 2000.
- Ziegler, J. F., J. P. Biersack, and V. Littmark, *The Stopping and Ranges of Ions in Solids*, Pergamon, New York, 1985.

D. Delcourt, Centre d'Etudes des Environnements Terrestre et Planétaires/IPSL, 94107 Saint Maur, France. (dominique.delcourt@cetp.ipsl.fr)
 R. E. Johnson, Engineering Physics Program, University of Virginia, Thornton Hall B103, Charlottesville, VA 22903, USA. (rej@virginia.edu)
 F. Leblanc, Service d'Aéronomie du CNRS/IPSL, BP 3 Reduit de Verrières, 91371 Verrières-Le-Buisson, France. (francois.leblanc@aerov.jussieu.fr)